




Article

Mcconnellite, CuCrO_2 and ellinaite, CaCr_2O_4 , from varicoloured spurrite marble of the Daba-Siwaqa area, Hatrurim Complex, Jordan

Irina O. Galuskina^{1*} , Marcin Stachowicz², Krzysztof Woźniak³, Yevgeny Vapnik⁴ and Evgeny Galuskin¹

¹Institute of Earth Sciences, Faculty of Natural Sciences, University of Silesia, Będzińska 60, 41-200 Sosnowiec, Poland; ²Institute of Geochemistry, Mineralogy and Petrology, University of Warsaw, Żwirki i Wigury 93, 02-089 Warszawa, Poland; ³Department of Chemistry, University of Warsaw, Pasteura 1, 02-093 Warszawa, Poland; and ⁴Department of Geological and Environmental Sciences, Ben-Gurion University of the Negev, P.O.B. 653, Beer-Sheva 84105, Israel

Abstract

A common attribute of two rare natural chromium-bearing oxides: mcconnellite, CuCrO_2 , discovered more than 40 years ago in Guyana, and a new mineral ellinaite, CaCr_2O_4 , described from two localities (Brazil and Israel) recently, is that these minerals are poorly studied due to their rarity and small size. Mcconnellite and ellinaite in the present study were found in varicoloured marbles of the pyrometamorphic Hatrurim Complex in the Tulul Al Hammam area, Daba-Siwaqa, Jordan. Structural data obtained for ellinaite ($Pnma$, $a = 9.0875(2)$, $b = 2.9698(1)$, $c = 10.6270(3)$ Å and $V = 286.80(2)$ Å³), with an empirical formula $(\text{Ca}_{1.00}\text{Sr}_{0.01})_{\Sigma 1.01}(\text{Cr}_{1.79}\text{Al}_{0.07}\text{Ca}_{0.04}\text{Fe}_{0.04}\text{Ti}_{0.03}^{4+}\text{Mg}_{0.03})_{\Sigma 2.00}\text{O}_4$, is similar to the structural data of synthetic analogue $\beta\text{-CaCr}_2\text{O}_4$ but differs significantly from the data obtained for ellinaite from Brazil and Israel despite the fact that all the natural phases have a similar composition. Single-crystal X-ray diffraction data for mcconnellite from Jordan ($R\bar{3}m$, $a = b = 2.9756(1)$ and $c = 17.124(1)$ Å) with composition $(\text{Cu}_{0.98}\text{Ca}_{0.03}\text{Sr}_{0.01})_{\Sigma 1.02}(\text{Cr}_{0.90}\text{Al}_{0.05}\text{Fe}_{0.03}^{3+})_{\Sigma 0.98}\text{O}_2$, is the first determination of a natural Cu-delafoosite-type structure. This paper also presents the results of a single-crystal Raman study for mcconnellite and ellinaite, which indicates that the spectral features of these minerals is dependent on crystal orientation.

Keywords: mcconnellite, ellinaite, delafossite, post-spinel, structure, Raman, Hatrurim Complex, Jordan

(Received 30 November 2020; accepted 11 March 2021; Accepted Manuscript published online: 17 March 2021; Associate Editor: G. Diego Gatta)

Introduction

Rare Cr-bearing oxides mcconnellite, CuCrO_2 , and ellinaite, $\beta\text{-CaCr}_2\text{O}_4$, were found in varicoloured marbles of the pyrometamorphic Hatrurim Complex in the Tulul Al Hammam area, Daba-Siwaqa, central Jordan in association with a recently discovered new garnet of the bitikleite group – priscillagrewite-(Y), $(\text{Ca}_2\text{Y})\text{Zr}_2\text{Al}_3\text{O}_{12}$ (Galuskina *et al.*, 2021). The results of previous investigations of both mcconnellite, described more than 40 years ago (Milton *et al.*, 1976), and a new mineral ellinaite (Sharygin, 2019; Sharygin *et al.*, 2020) allow for some important questions to be made.

Mcconnellite (CuCrO_2 , $R\bar{3}m$, $a = b = 2.983(4)$ Å, $c = 17.16(3)$ Å) was known from only one locality – Merume River, Kamakusa, Potaro-Siparuni Region, Guyana, in hydrothermal Cr-bearing ore, so called, ‘merumite’ type (Milton *et al.*, 1976). The mcconnellite description contains incomplete chemical data and its identification was based on a few lines from a diffraction pattern coinciding with the lines of a synthetic analogue (Milton *et al.*, 1976). Mcconnellite was simultaneously described in association with three other new minerals: grimaldiite, $\alpha\text{-CrOOH}$; guyanaite, $\beta\text{-CrOOH}$; and bracewellite, $\gamma\text{-CrOOH}$ (Milton *et al.*, 1976).

Mcconnellite, according to the authors’ opinion, occurs in epitaxial intergrowth with isostructural grimaldiite, $\alpha\text{-CrOOH}$ ($R\bar{3}m$, $a = b = 2.973(2)$ and $c = 13.39(1)$ Å), forming zones unevenly enriched in Cu to ~ 10 μm in thickness in grimaldiite (Milton *et al.*, 1976). A phase similar to mcconnellite has been identified in a historical Cu–Pb-slag from Tsumeb, Namibia (Ettler *et al.*, 2009). Recently, synthetic CuCrO_2 and other materials with a delafossite-type structure have been studied extensively because of their thermoelectric, optoelectric, electric, magnetic and superconductor properties (Kumar *et al.*, 2012; Monteiro *et al.*, 2017; Majee and Bhowe, 2020). Synthetic delafossite with the general formula $\text{CuR}^{3+}\text{O}_2$ is prepared at different temperatures by performing a solid-state reaction, usually at temperatures $>850^\circ\text{C}$, by the sol-gel method, with a high-temperature post treatment ($>650^\circ\text{C}$) or by hydrothermal synthesis at 180°C (Kim *et al.*, 2020).

Ellinaite is a new mineral, approved in 2020, was described from two localities and studied using only a few grains: a μm -sized inclusion in diamond from Brazil (co-type, Kaminsky *et al.*, 2015) and inclusions of 20 μm in pyrrhotite from gehlenite-bearing breccia with phosphides (holotype; Sharygin 2019; Sharygin *et al.*, 2020). A large specimen of gehlenite-bearing breccia was found *ex situ* by Mikhail Murashko in 2005 at the dry Zohar Wadi in the Negev Desert (Hatrurim Basin), Israel (Galuskin *et al.*, 2020). The small size and limited amount of materials did not allow for investigation into the detailed physical properties and to also accurately determine structural parameters

*Author for correspondence: Irina O. Galuskina, Email: irina.galuskina@us.edu.pl

Cite this article: Galuskina I.O., Stachowicz M., Woźniak K., Vapnik Y. and Galuskin E. (2021) Mcconnellite, CuCrO_2 and ellinaite, CaCr_2O_4 , from varicoloured spurrite marble of the Daba-Siwaqa area, Hatrurim Complex, Jordan. *Mineralogical Magazine* 85, 387–397. <https://doi.org/10.1180/mgm.2021.27>

Table 1. Chemical composition (wt.%) of ellinaite from Jordan.

	<i>n</i> = 10	S.D.	Range	Calculated on 40	
TiO ₂	1.27	0.40	0.79–2.06	Ti	0.03
Fe ₂ O ₃	1.43	0.35	1.17–2.14	Fe ³⁺	0.04
Cr ₂ O ₃	65.44	0.81	63.74–66.43	Cr ³⁺	1.79
Al ₂ O ₃	1.71	0.07	1.60–1.82	Al	0.07
SrO	0.54	0.04	0.49–0.62	Sr	0.01
CaO	27.95	0.16	27.70–28.23	Ca	1.04
MgO	0.62	0.13	0.43–0.83	Mg	0.03
Total	98.96				

S.D. – standard deviation

Table 2. Chemical composition (wt.%) of mcconnellite from Jordan.

	<i>n</i> = 8	S.D.	Range	Calculated on 20	
Cu ₂ O	47.36	0.49	46.78–48.03	Cu ¹⁺	0.98
SrO	0.47	0.03	0.42–0.50	Sr	0.01
CaO	1.27	0.15	1.04–1.53	Ca	0.03
MgO	0.06	0.04	0.02–0.12	Sum A	1.02
Al ₂ O ₃	1.64	0.19	1.16–1.78	Al	0.05
Fe ₂ O ₃	1.43	0.28	1.20–2.13	Fe ³⁺	0.03
Cr ₂ O ₃	46.32	0.41	45.63–47.14	Cr ³⁺	0.90
Total	98.55			Sum B	0.98

S.D. – standard deviation

of ellinaite from this occurrence (Kaminsky *et al.*, 2015; Sharygin, 2019; Sharygin *et al.*, 2020). For ellinaite from Israel, the following structural data were obtained: an orthorhombic crystal system, *Pnma* space group, $a = 8.868(9)$, $b = 2.885(3)$, $c = 10.355(11)$ Å and $V = 264.9(5)$ Å³ (Sharygin *et al.*, 2020). The cell parameters of the ellinaite inclusion in diamond were obtained based on electron diffraction (HRTEM): orthorhombic, *Pnma*, $a = 9.017$, $b = 2.874$, $c = 10.170$ Å and $V = 263.6$ Å³ (Kaminsky *et al.*, 2015). These parameters differ distinctly from the cell parameters obtained by us for ellinaite from a new location in Jordan: *Pnma*, $a = 9.0875(2)$, $b = 2.96980(10)$, $c = 10.6270(3)$ Å and $V = 286.80(2)$ Å³, which are close to the parameters of the synthetic β-CaCr₂O₄ (*Pnam*, $a = 9.083(2)$, $b = 10.629(2)$, $c = 2.971(1)$ Å and $V = 286.8(1)$ Å³, Zhai *et al.*, 2016). The chemical composition and Raman spectroscopy data of Israeli ellinaite (Sharygin, 2019) prove that this is a natural analogue of β-CaCr₂O₄.

In the present paper, we provide new data on the composition and structure on mcconnellite and ellinaite from Jordan. In addition, novel Raman data are provided, together with optical images of these minerals showing their real colour, which is also diagnostic property.

Methods of investigation

Composition and morphology

The morphology and composition of ellinaite, mcconnellite and associated minerals (Tables 1,2,3) were studied using optical microscopy and scanning electron microscopes (Phenom XL and PhilipsXL30/EDAX, Institute of Earth Sciences, Faculty of Natural Sciences, University of Silesia, Sosnowiec, Poland) and electron microprobe analysis (Cameca SX100, Institute of Geochemistry, Mineralogy and Petrology, University of Warsaw, Warszawa, Poland). Chemical analyses were carried out in the WDS-mode (wavelength-dispersive X-ray spectroscopy, settings:

Table 3. Chemical composition of minerals associated with ellinaite and mcconnellite: cuprite and Cr-spinel (core – zincchromite, rim – magnesiochromite).

	Cuprite		Cr-spinel	
	<i>n</i> = 2	Zincchromite <i>n</i> = 3	Magnesiochromite <i>n</i> = 3	
Wt.%				
TiO ₂	n.d.	0.31	n.d.	
Fe ₂ O ₃	n.d.	3.43	1.87	
Cr ₂ O ₃	0.32	53.16	63.85	
Al ₂ O ₃	n.d.	9.83	7.18	
SrO	n.d.	0.52	0.60	
ZnO	n.d.	20.95	7.82	
CaO	1.06	1.22	1.04	
MgO	n.d.	9.63	15.72	
Cu ₂ O	97.23	n.d.	n.d.	
Total	98.61	99.04	98.07	
Atoms per formula unit				
Calculated on	20	30	30	
Cu ¹⁺	1.97			
Mg		0.49	0.77	
Zn		0.54	0.20	
Ca	0.03	0.04	0.04	
Sr		0.01	0.01	
Sum R ²⁺		1.08	1.02	
Cr ³⁺	0.01	1.44	1.66	
Al		0.40	0.28	
Fe ³⁺		0.09	0.05	
Sum R ³⁺		1.93	1.99	
Ti ⁴⁺		0.01		

n.d. – not detected

15 keV, 10 nA and ~1 μm beam diameter) using the following lines and standards: CaKα and MgKα – diopside, AlKα – orthoclase, TiKα – rutile, FeKα – Fe₂O₃, SrLα – celestine, CuKα – cuprite, ZnKα – sphalerite and CrKβ – Cr₂O₃. Contents of other chemical elements, including some of those determined in the holotype ellinaite i.e. Na, V and Mn, are below the detection limit.

Raman spectroscopy

Raman spectra of ellinaite and mcconnellite were recorded on a WITec alpha 300R Confocal Raman Microscope (Institute of Earth Science, Faculty of Natural Sciences, University of Silesia, Sosnowiec, Poland) equipped with an air-cooled solid-state laser (488 nm) and a charge-coupled device (CCD) camera operating at –61°C. An air Zeiss LD EC Epiplan-Neofluar DIC-100/0.75NA objective (Carl Zeiss AG, Jena, Germany) was used. Raman scattered light was focused on a broadband single-mode fibre with an effective pinhole size of ~30 μm and a monochromator with a 600 g/mm⁻¹ grating was used. The power of the laser at the sample position was *ca.* 20 mW. Integration times of 5 s with an accumulation of 20 scans and a resolution 3 cm⁻¹ were chosen. The monochromator was calibrated using the Raman scattering line of a silicon plate (520.7 cm⁻¹).

X-ray diffraction and crystal structure determination

X-ray data were collected at the University of Warsaw Biological and Chemical Research Centre, using an SuperNova four-circle

Table 4. Crystal data, X-ray measurement and refinement parameters for ellinaite and mcconnellite.

	Ellinaite	Mcconnellite
Crystal data		
Crystal dimensions (mm)	0.018 × 0.01 × 0.008	0.028 × 0.01 × 0.007
Crystal system, space group	Orthorhombic, <i>Pnma</i>	Trigonal, $R\bar{3}m$
Temperature (K)	293	293
<i>a</i> , <i>b</i> , <i>c</i> (Å)	9.0875(2), 2.9698(1), 10.6270(3)	2.9756(1), 2.9756(1), 17.1244(10)
<i>V</i> (Å ³)	286.80(2)	131.31(1)
<i>Z</i>	4	3
Calculated density (g cm ⁻³)	4.609	5.311
μ (mm ⁻¹)	8.15	16.35
Data collection		
Crystal description	Tabular	Irregular
Instrument	Rigaku Oxford Diffraction SuperNova, Eos CCD	
Radiation type, wavelength (Å)	MoK α , 0.71073	
Number of frames	2096	856
2 θ range (°)	5.898 to 67.64	7.138 to 67.168
Absorption correction	Gaussian	Gaussian
T_{\min} , T_{\max}	0.867, 0.938	0.657, 0.894
No. of measured, independent and observed [<i>I</i> > 4 σ (<i>I</i>)] reflections	15823, 660, 642	1045, 90, 88
R_{int}	0.0495	0.0208
Data completeness to 25.242° θ (%)	100	100
Indices range of <i>h</i> , <i>k</i> , <i>l</i>	-13 ≤ <i>h</i> ≤ 14, -4 ≤ <i>k</i> ≤ 4, -16 ≤ <i>l</i> ≤ 16	-4 ≤ <i>h</i> ≤ 4, -4 ≤ <i>k</i> ≤ 4, -25 ≤ <i>l</i> ≤ 25
Refinement details		
Refinement	Full-matrix least squares on F^2	Full-matrix least squares on F^2
Number of reflections, parameters, restraints	660, 46, 0	90, 10, 0
R_1 [<i>I</i> > 2 σ (<i>I</i>)], R_1 (all)	0.022, 0.0235	0.0144, 0.0149
wR_2 [<i>I</i> > 2 σ (<i>I</i>)], wR_2 (all)	0.0373, 0.0375	0.0266, 0.0267
GoF	1.291	1.143
$\Delta\rho_{\max}$, $\Delta\rho_{\min}$ (e ⁻ Å ⁻³)	0.45, -0.69	0.33, -0.61

diffractometer equipped with an EOS CCD detector (Rigaku Oxford Diffraction), the detector-to-crystal distance was 45.8 mm. MoK α radiation ($\lambda = 0.71073$ Å) was used at 50 kV and 0.8 mA. Ellinaite and mcconnellite structures are refined based on diffraction data collected on crystals $7 \times 10 \times 28$ μm and $8 \times 10 \times 18$ μm , respectively (Table 4). Composition and Raman spectra were measured on the same crystals. A frame-width of 1° in ω scans and a frame time of 240 s and 100 s were used for mcconnellite and ellinaite, respectively. The full Ewald sphere was collected up to $\theta = 34^\circ$ with R_{int} values of 0.0208 for mcconnellite and up to 32° with $R_{\text{int}} = 0.0495$ for ellinaite. Reflection intensities were corrected for Lorentz, polarisation and absorption effects and converted to structure factors using *CrysalisPro*® software (Rigaku-Oxford Diffraction). A numerical absorption correction based on Gaussian integration over a multifaceted crystal model was used. The crystallographic information files of both minerals have been deposited with the Principal Editor of *Mineralogical Magazine* and are available as Supplementary material (see below). Fractional atomic coordinates and displacement parameters, selected bond distances and bond valence sums (BVS)

for ellinaite are given in Tables 5–7 and for mcconnellite in Tables 8–10. Both structures were solved with a dual-space iterative phasing algorithm implemented in *ShelXT* (Sheldrick, 2015a) that located all the positions of cations (all labelled as Ca) and O anions. Correct element assignment for cations was based upon compositional data obtained by electron microprobe analysis (EMPA) and crystal-chemical reasoning, comprising site-scattering, coordination and bond lengths. The model was refined with the least squares minimisation using *Shelxl* (Sheldrick, 2015b), within *Olex2* (Dolomanov *et al.*, 2009) as the graphical interface. When more than one element occupies the same position in the asymmetric unit, constraints for equal atom coordinates and equal anisotropic displacement parameters for these groups of atoms within each unique site were applied. The occupancies of $M1$ and $M2$ in ellinaite (Table 5) and M in mcconnellite (Table 8), were constrained to 1 and refined as $M1(\text{Cr vs. Al})$, $M2(\text{Cr vs. Mg})$ and $M(\text{Cr vs. Al})$. The A site (ellinaite, Table 5) and Q site (mcconnellite, Table 8) were refined as fractional occupancy of $^A\text{Ca vs. vacancy}$ (\square) and fractional occupancy of $^Q\text{Cu vs. } \square$, respectively.

Table 5. Fractional atomic coordinates and displacement parameters (Å²) for ellinaite.

	<i>x/a</i>	<i>y/b</i>	<i>z/c</i>	U_{eq}	U^{11}	U^{22}	U^{33}	U^{13}
A*	0.74117(7)	¼	0.15888(6)	0.00746(15)	0.0073(3)	0.0072(3)	0.0080(3)	0.0000(2)
M1*	0.41700(6)	¾	0.10128(5)	0.00270(13)	0.0026(2)	0.0030(2)	0.0025(2)	-0.0001(17)
M2*	0.56045(6)	¼	0.38769(5)	0.00238(13)	0.0022(2)	0.0027(2)	0.0022(2)	0.0010(16)
O1	0.6169(3)	¾	0.0237(2)	0.0042(4)	0.0041(9)	0.0042(11)	0.0044(9)	0.0004(7)
O2	0.5817(3)	¼	0.5734(2)	0.0045(4)	0.0040(9)	0.0052(11)	0.0041(9)	-0.0005(7)
O3	0.2033(3)	¾	0.1600(2)	0.0053(4)	0.0043(9)	0.0044(11)	0.0073(10)	-0.0001(8)
O4	0.4734(3)	¼	0.2147(2)	0.0050(4)	0.0071(10)	0.0050(11)	0.0029(9)	-0.0009(8)

$U^{12} = U^{23} = 0$ for all atoms

*Refined fractional Cr vs. Al occupancies at M1 is $x\text{Cr} = 0.833(18)$; for Cr vs. Mg at M2 is $x\text{Cr} = 0.858(8)$; for Ca vs. \square at A is $x\text{Ca} = 0.965(4)$

Table 6. Selected bond distances (Å) of ellinaite.

M1–O1	1.9946(15)	M2–O2	2.0114(10) ×2
M1–O1	2.0161(10) ×2	M2–O2	1.9835(15)
M1–O3	2.0386(15)	M2–O3	2.0377(10) ×2
M1–O4	1.9803(10) ×2	M2–O4	2.0005(15)
<M1–O>	2.004	<M2–O>	2.014
A–O1	2.3548(12) ×2		
A–O2	2.3704(12) ×2		
A–O3	2.4540(12) ×2		
A–O4	2.5026(16)		
A–O4	2.5032(16)		
<A–O>	2.421		

Table 7. Bond-valences⁺ and bond-valence sums (BVS) in valence units for ellinaite.

	O1	O2	O3	O4	BVS	Cations*
^{M1} Cr	0.45 ^{x21} ×2→, 0.48		0.43	0.50 ^{x21} ×2→	2.82	2.76
^{M2} Cr		0.46 ^{x21} , 0.50	0.43 ^{x21}	0.47	2.75	2.69
^A Ca	0.35 ^{x21}	0.34 ^{x21}	0.27 ^{x21}	0.23 ^{x21}	2.38	
BVS	2.09	2.09	1.82	1.94		
Anions*	2.06	2.06	1.79	1.91		

⁺Calculated using the bond-valence parameters of Brown and Altermatt (1985)

*Calculated using occupancies assigned from EMPA for M1, M2, equally distributed for both sites

Occurrence and material description

Mcconnellite and ellinaite were found in a sample of spurrite marble (Fig. 1a) collected from one of quarries (31°32'31"N, 36°10'19"E) in the Tulul Al Hammam area, which is in the pyrometamorphic field of the Daba-Siwaqa area, central Jordan. The varicoloured marble belongs to the upper part of the Maastrichtian–Paleogene Muwaqqar Chalk–Marl Unit (Khoury et al., 2016; Sokol et al., 2017; Khoury, 2020). This unit was transformed to varicoloured marble by pyrometamorphism, and is, therefore, included in the Hatrurim Complex (Mottled Zone of Picard, 1931). The Daba–Siwaqa area embraces numerous outcrops of the Hatrurim Complex rocks located on the Transjordan plateau south of Amman (Novikov et al., 2013; Khoury et al., 2016; Khoury, 2020).

The sample of spurrite marble shown in Fig. 1a contains green zones enriched in fluorapatite crystals. In these zones a new garnet, priscillagrewite-(Y), {Ca₂Y}[Zr₂](Al₃)O₁₂ has been found (Galuskina et al., 2021). In the brown part of the marble, whose colour is mainly caused by minerals of the brownmillerite–srebrodolskite series (Fig. 1a), mcconnellite and ellinaite crystals are present near a channel filled with later ettringite (Fig. 1b). In spurrite marble, besides calcite, spurrite, fluorapatite, minerals of the

Table 9. Selected bond distances (Å) for mcconnellite.

Q (Cu)–O1	1.847(2) ×2
M (Cr)–O1	1.9914(10) ×6

Table 10. Bond-valences⁺ and bond-valence sums (BVS) in valence units for mcconnellite.

	O	BVS	Cations*
^M Cr	0.49 ^{x31} ×6→	2.91	2.84
^Q Cu	0.53 ^{x2} →	1.05	
BVS	1.98		
Anions*	1.95		

⁺Calculated using the bond-valence parameters of Brown and Altermatt (1985)

*Calculated using occupancies assigned from EMPA for M.

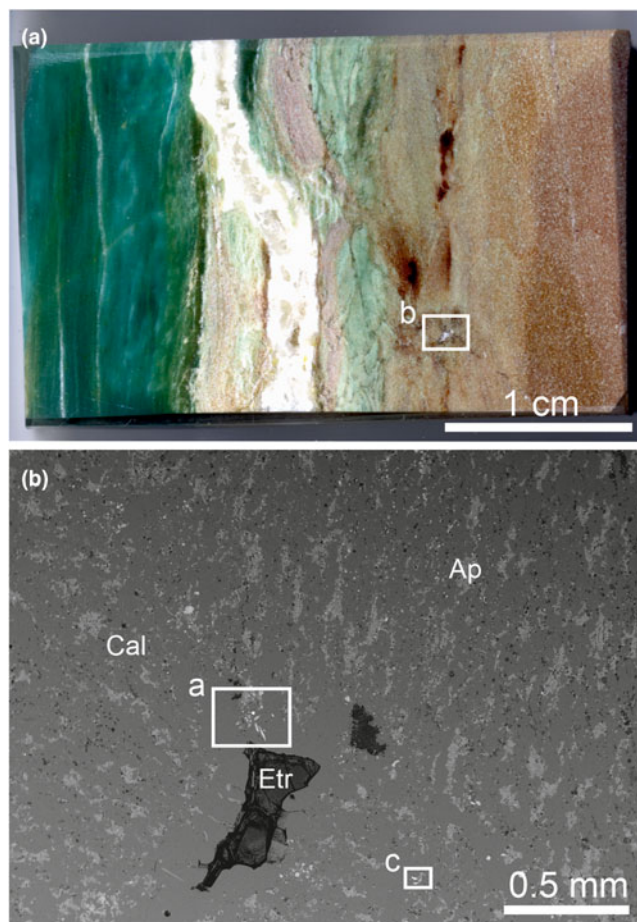


Fig. 1. (a) Polished section of varicoloured marble, in which in brown calcite zone mcconnellite and ellinaite were found and the green fluorapatite zone in which priscillagrewite-(Y) was detected. The white frame shows the area magnified in Fig. 1b. (b) Channel in marble of partially infilled ettringite, near which ellinaite (frame a) and mcconnellite (frame c) occur. Fragments in frames are magnified in Fig. 2a and 2c, respectively. Ap = fluorapatite, Etr = ettringite and Cal = calcite.

Table 8. Atom coordinates, equivalent-isotropic and anisotropic displacement parameters (Å²) of mcconnellite.

	x/a	y/b	z/c	U _{eq}	U ¹¹	U ²²	U ³³	U ¹²
Q*	2/3	1/3	1/3	0.00937(16)	0.01145(19)	0.01145(19)	0.0052(2)	0.00572(10)
M*	1/3	2/3	1/6	0.00387(18)	0.0032(2)	0.0032(2)	0.0052(3)	0.00160(11)
O	2/3	1/3	0.22548(11)	0.0071(5)	0.0069(6)	0.0069(6)	0.0074(9)	0.0034(3)

U¹³=U²³=0 for all atoms

*Refined fractional Cr vs. Al occupancies at M is xCr = 0.833(18); for Cu vs. □ at Q is xCu = 0.946(8)

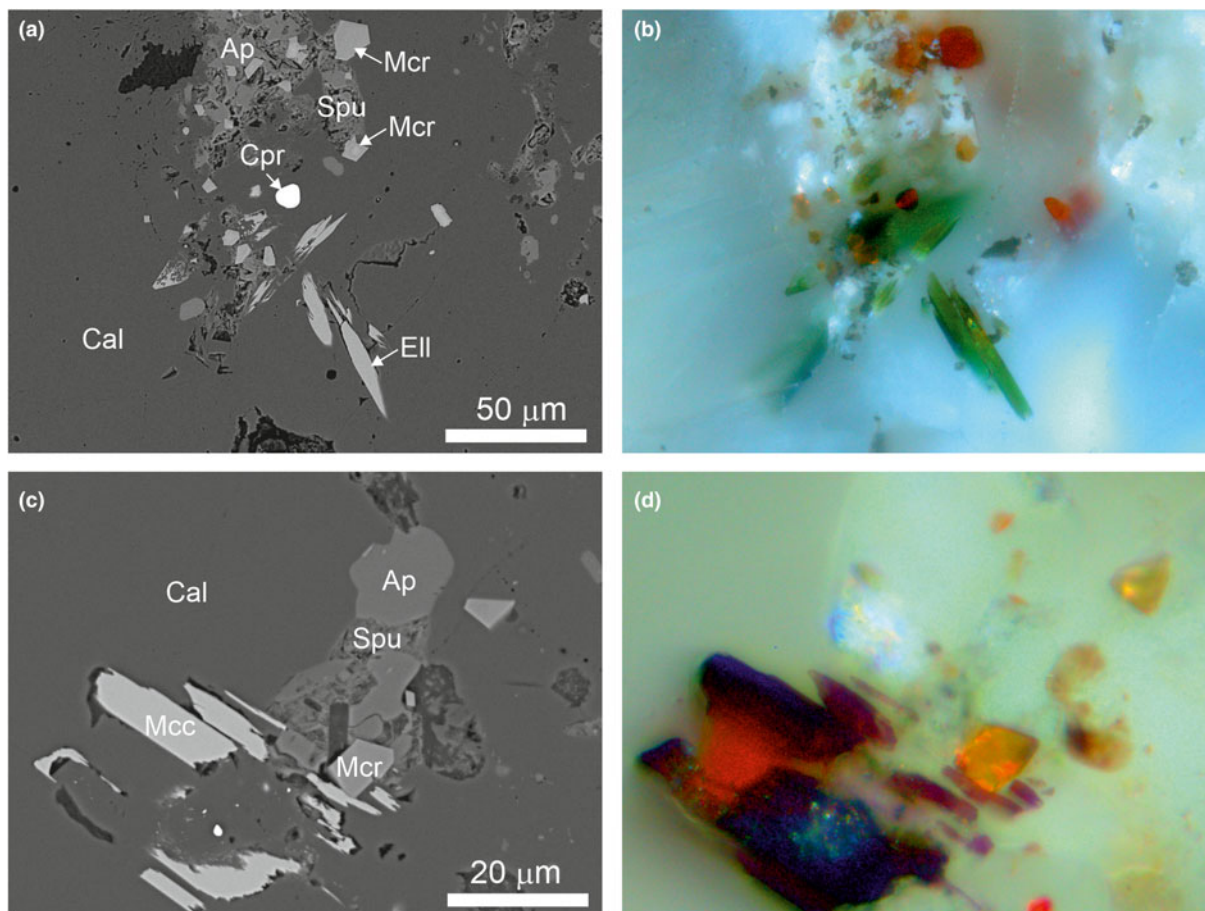


Fig. 2. (a, b) Ellinaite associated with minerals of the magnesiochromite-zincochromite series and cuprite. (a) Back-scattered electron image, (b) optical image – the characteristic bright-green colour of ellinaite is visible. (c, d) Series of sub-parallel mcconnellite crystals. (c) BSE image, (d) optical image – the characteristic purple colour of mcconnellite is visible in thin crystals. Ap = fluorapatite, Cal = calcite, Cpr = cuprite, Ell = ellinaite, Mcr = magnesiochromite-zincochromite and Mcc = mcconnellite.

brownmillerite–srebrodolskite series and priscillagrewite-(Y), the following accessory minerals are found: fluormayenite, lakargiite, baghdadite, hematite, sphalerite, zincite, garnet of the andradite-grossular series, tululite, vapnikite, minerals of the lime–montepionite and magnesiochromite–zincochromite series, cuprite and Y-bearing and Y-free perovskite (Galuskina *et al.*, 2021). Cuprite contains Cr and Ca impurities (Table 3). Zincochromite ($\text{ZnCr}_2\text{O}_4 \approx 54\%$) is the predominant end-member in the core of Cr-bearing spinel, the rim is composed of magnesiochromite ($\text{MgCr}_2\text{O}_4 \approx 77\%$; Table 3).

Elongated crystals of ellinaite up to 40 μm in length, and up to 8 μm in width have a bright-green colour, and occur in calcite (Fig. 2a, b). Ellinaite from Jordan has Ti^{4+} , Fe^{3+} , Al, Sr and Mg impurities and slightly enhanced Ca content in comparison with the ideal formula (Table 1). The empirical formula of ellinaite calculated on 4 oxygens is: $(\text{Ca}_{1.00}\text{Sr}_{0.01})_{\Sigma 1.01}(\text{Cr}_{1.79}\text{Al}_{0.07}\text{Fe}_{0.04}\text{Ca}_{0.04}\text{Ti}_{0.03}\text{Mg}_{0.03})_{\Sigma 2.00}\text{O}_4$, which gives a CaCr_2O_4 end-member content of $\sim 90\%$. Ellinaite from inclusions in diamond (co-type) also has slight non-stoichiometry: $(\text{Ca}_{0.97}\text{Mg}_{0.02}\text{Mn}_{0.02})_{\Sigma 1.01}(\text{Cr}_{1.71}\text{Ca}_{0.11}\text{Fe}_{0.06}\text{V}_{0.06}\text{Ti}_{0.03}\text{Al}_{0.03})_{\Sigma 2.00}\text{O}_4$ (Kaminsky *et al.*, 2015). Sharygin (2019) assigned the crystal chemical formula: $(\text{Ca}_{0.967}\text{Fe}_{0.017}\text{Na}_{0.010})_{\Sigma 0.994}(\text{Cr}_{1.696}\text{V}_{0.201}\text{Ti}_{0.080}\text{Al}_{0.024}\text{Ti}_{0.005})_{\Sigma 2.006}\text{O}_4$, to ellinaite from phosphide-bearing rock (holotype), balancing a charge excess by Ti^{3+} (Sharygin, 2019). This ellinaite is characterised by relatively high V content.

Mcconnellite forms a series of parallel crystals in calcite, the largest of which is $\sim 20 \mu\text{m}$ long and $10 \mu\text{m}$ thick (Fig. 2c). Mcconnellite in thin crystals shows a characteristic purple colour (Fig. 2d). The mcconnellite studied from Jordan has the crystal chemical formula $(\text{Cu}_{0.98}\text{Ca}_{0.03}\text{Sr}_{0.01})_{\Sigma 1.02}(\text{Cr}_{0.90}\text{Al}_{0.05}\text{Fe}_{0.03})_{\Sigma 0.98}\text{O}_2$, that corresponds to 90% of the end-member CuCrO_2 (Table 2). Accurate data on the holotype mcconnellite composition from Guyana are absent (Milton *et al.*, 1976).

Raman spectroscopy data of ellinaite and mcconnellite

The spectral features of both ellinaite and mcconnellite are dependent on the crystal orientation (Figs 3, 4). Raman spectra of ellinaite from Jordan are similar to the spectra of the holotype ellinaite from Israel (Sharygin, 2019) and its synthetic analogue (Zhai *et al.*, 2016). The main bands in the Raman spectrum of ellinaite are the following [Fig. 3a, interpretation by analogy with harmunite, CaFe_2O_4 (Kolev *et al.*, 2003; Galuskina *et al.*, 2014)]: a series of bands in the range $1400\text{--}1200 \text{ cm}^{-1}$ [combination of first-order phonons Ag (701 cm^{-1}) + Ag (598 cm^{-1}), $2 \times \text{Ag}$ (701 cm^{-1}), $2 \times \text{Ag}$ (598 cm^{-1})]; $701, 598, 558 \text{ cm}^{-1}$ (Ag , stretching modes); $488, 473, 448 \text{ (B2g/Ag, bending and tilting modes)}$; $393, 344, 327 \text{ (Ag/B1g/B3g, rotation mode)}$; $249, 212, 198 \text{ (Ag)}$, $141 \text{ (Ag, Ca-related vibration)}$. The main band at 598 cm^{-1} in the Raman spectrum of ellinaite is related to symmetric vibrations

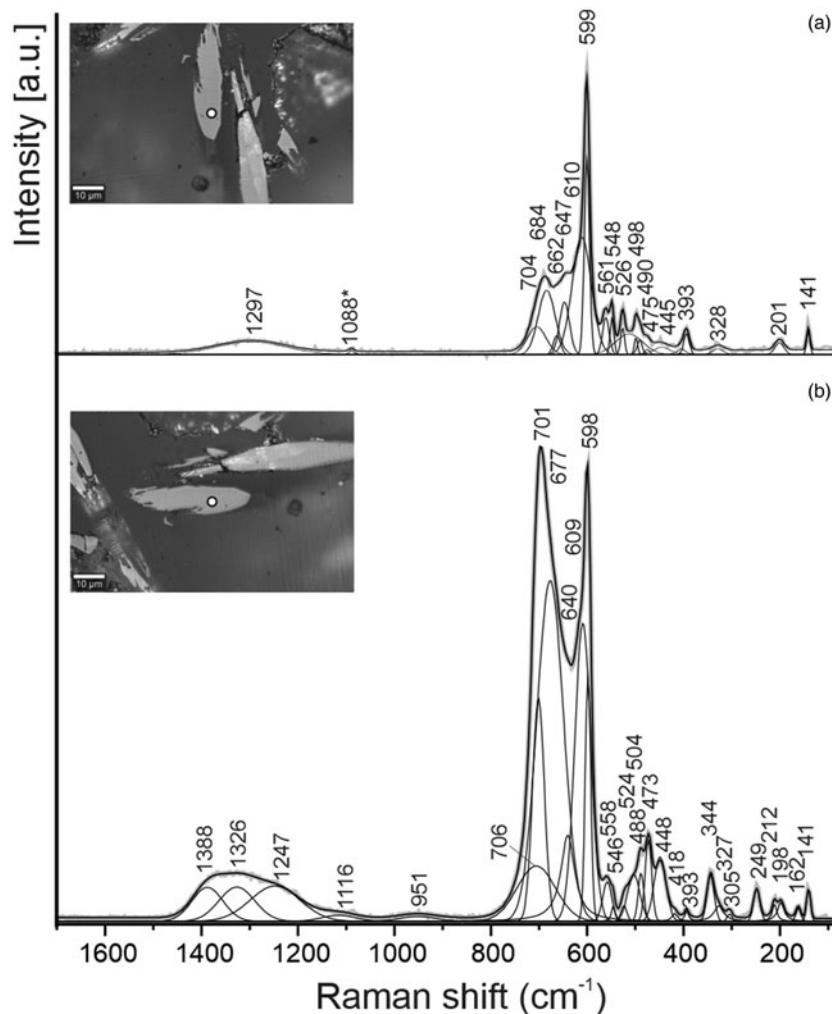


Fig. 3. Raman spectra of ellinaite obtained in a random section at the two orientations relative to a polarised laser beam. The point location for the spectra is shown as white circles in the inset optical images.

of Cr–O in octahedron, in the eskolaite Cr_2O_3 spectrum the analogous band is at a lower frequency – 548 cm^{-1} (Shim *et al.*, 2004). The band at $\sim 700\text{ cm}^{-1}$ in the ellinaite spectrum is polarised and has large full widths at half maximum and a complex nature (Fig. 3). It is probably attributed to symmetric vibrations in the Cr–O–Cr group and asymmetric vibrations of Cr–O.

For the first time we provide the Raman spectra of mcconnellite (Fig. 4), which are similar to the spectra of synthetic CuCrO_2 , for which depending on orientation and/or composition modification significant changes of intensity of the main bands are observed (Aktas *et al.*, 2012; Elkhouni *et al.*, 2013; Monteiro *et al.*, 2017, 2018; Han *et al.*, 2020). In the Raman spectra of mcconnellite there are six main bands (Fig. 4b, cm^{-1}): 105, 210 (Ag), 458 (Eg), 538 (P_1), 556 (P_1') and 709 (A_{1g}) (Monteiro *et al.*, 2018). The nature of the strong band at 538 cm^{-1} (P_1) and the shoulder at 556 cm^{-1} (P_1') is currently disputable and is connected with structural defects of mcconnellite, which interferes with an action of the Raman selection rule (Majee and Bhohe, 2020; Han *et al.*, 2020).

Crystal structure of ellinaite and mcconnellite

Ellinaite from Jordan, CaCr_2O_4 (*Pnma*, $a = 9.0875(2)$, $b = 2.9698(1)$, $c = 10.6270(3)\text{ \AA}$ and $V = 286.80(2)\text{ \AA}^3$), belongs to the post-spinel of the CF (calcium ferrite) structural type. Harmunite, CaFe_2O_4

(*Pnma*; $a = 9.2183(3)$, $b = 3.0175(1)$, $c = 10.6934(4)\text{ \AA}$, $Z = 4$ and $V = 297.45(2)\text{ \AA}^3$), described from Iarnite rocks of the Hatrum Complex, Jabel Harmun, Palestine (Galuskina *et al.*, 2014) and wernerkrauseite with the defect structure, $\text{Ca}_{2/3}(\text{Fe}_{4/3}^{3+}\text{Mn}_{2/3}^{4+})_{\Sigma 2}\text{O}_4$ (*Pnma*, $a = 9.0548(2)$, $b = 2.8718(1)$, $c = 10.9908(2)\text{ \AA}$ and $V = 285.80(1)\text{ \AA}^3$), found in altered xenoliths within alkaline basalts of the Bellerberg volcano, Eifel, Rhineland-Palatinate, Germany (Galuskin *et al.*, 2016) are the natural low-pressure and high-temperature members of CF-type ferrites. The ellinaite structure is composed of two types of symmetrically independent distinct corner sharing (Cr^{3+}O_6) distorted octahedra. Each of these octahedra forms double chains ${}_{\infty}[\text{Cr}_2\text{O}_6]_n$, linked by shared edges in a rutile-type manner (Fig. 5). The double chains connect together by common oxygen corners and build a tunnel-framework with large trigonal prismatic cavities occupied by Ca along [010] (Fig. 5). Octahedra (Cr^{3+}O_6) forming rutile-like chains in ellinaite are distorted with average distances ${}^{M1}\text{Cr}-\text{O} = 2.004(3)\text{ \AA}$ and ${}^{M2}\text{Cr}-\text{O} = 2.014(3)\text{ \AA}$ (Table 6). These values are slightly higher, than the Cr–O distance of 1.98 \AA , calculated for ideal octahedron (Shannon, 1976), and are caused by substitutions of other elements in M1, M2 crystallographic sites.

Mcconnellite from Jordan, CuCrO_2 ($R\bar{3}m$, $a = b = 2.9756(1)$ and $c = 17.124(1)\text{ \AA}$) is a structural analogue of delafossite, CuFeO_2 ($R\bar{3}m$, $a = b = 3.03\text{ \AA}$ and $c = 17.09\text{ \AA}$, Pabst, 1946). Dannhauser and Vaughan (1955) described synthetic cuprous

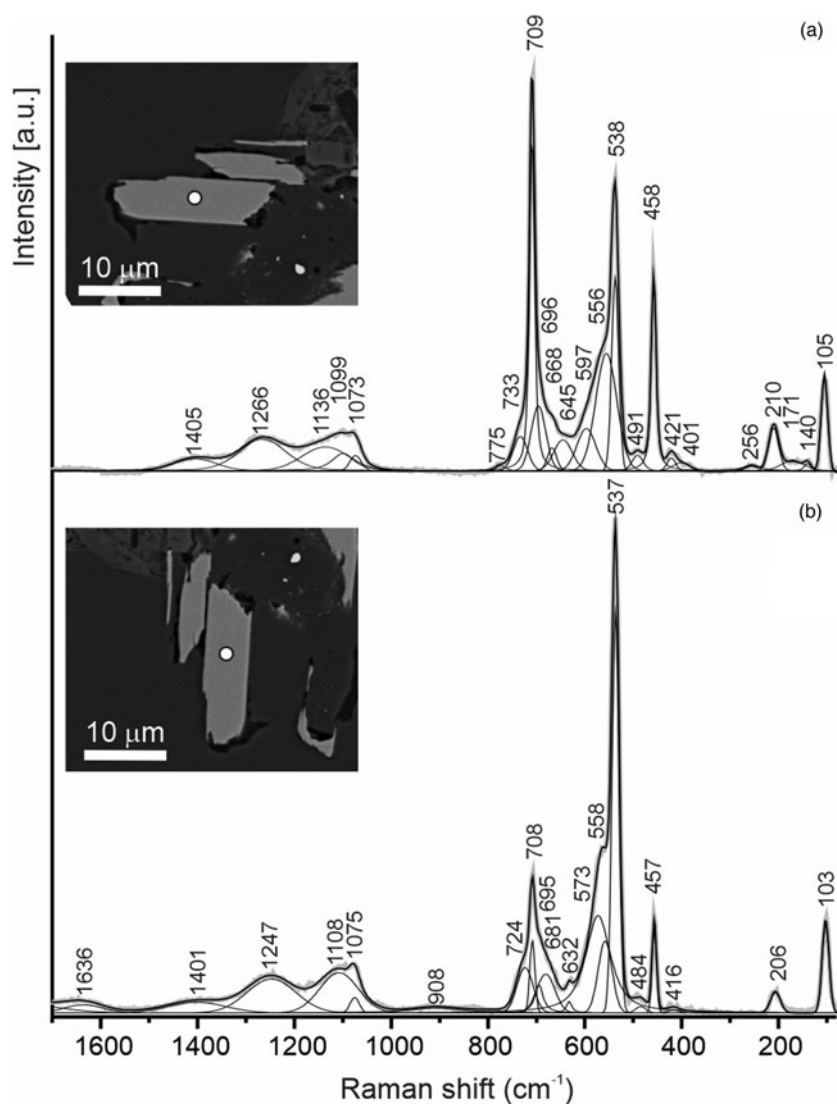


Fig. 4. Raman spectra of mcconnellite obtained at different orientations of the crystal. The point location for the spectra is shown as white circles in the inset BSE image.

chromite to the same space group after Stroupe (1949) who identified identical unit cell parameters though with a hexagonal primitive cell instead of rhombohedral. The mcconnellite crystal structure consists of distorted (Cr^{3+}O_6) octahedra with a Cr–O distance of 1.991(1) Å. Each octahedron shares six edges with six neighbours, forming (CrO_2)[−] infinite layers. Every two adjacent layers are linked by linear two-fold coordinated Cu^+ ions, forming (O–Cu–O)^{3−} groups. Copper (I) forms a hexagonal plane where each ion is 2.9756(1) Å away from the six neighbours. The $\text{Cu}^+–\text{Cu}^+$ distance determines the length of the unit cell parameter *a*. The (CrO_2)[−] layers and Cu^+ planes are perpendicular to the *z* axis and alternate along it (Fig. 6).

Discussion

Recent investigations have shown that Fe^{3+} -analogues of ellinaite and mcconnellite: harmunite, CaFe_2O_4 (Galuskina *et al.*, 2014) and delafossite, CuFeO_2 (Galuskina *et al.*, 2015; Krzatala *et al.*, 2018), respectively, are relatively widely distributed in pyrometamorphic rocks of the Hatrurim Complex. Areas of high chromium occur locally in the Complex, and Cr is found in the composition of the primary high-temperature pyrometamorphic

oxide minerals such as spinel, oxy-deficient perovskite of the brownmillerite–srebrodolskite and shulamitite–sharyginite series and other ferrites. Rarer high chromium contents are noted in Ti-bearing andradite and pyrrhotite (Sharygin *et al.*, 2013; Galuskina *et al.*, 2014, 2017; Juroszek *et al.*, 2018a). Low-temperature hydrothermally altered products of chromium-bearing pyrometamorphic rocks contain minerals of the hashemite–baryte and bentorite–ettringite–siwaqaite series (Seryotkin *et al.*, 2019; Juroszek *et al.*, 2018b, 2020a, 2020b), and also chromatite (Sokol *et al.*, 2011).

Varicoloured apatite–spurrite marbles of the pyrometamorphic complex are characterised by a very high chemical inhomogeneity. This is reflected not only in mineral composition and the colour of the rocks inherited in the primary layering of the protolith (Fig. 1a), but also in enrichment of separate micro-layers by various rare and accessory minerals (Khoury *et al.*, 2016; Galuskina *et al.*, 2021). In the sample studied (Fig. 1a), in the green apatite zone, a new Zr–Y(+REE) garnet – priscillagrewite–(Y) was found (Galuskina *et al.*, 2021); whereas in the spurrite zone, Cr and Cu oxides were noted (Figs 1b, 2). A source of Zr and Y is proposed as detrital minerals of primary sedimentary rocks (zircon), and Cr is connected with organic matter in the oil shales in the

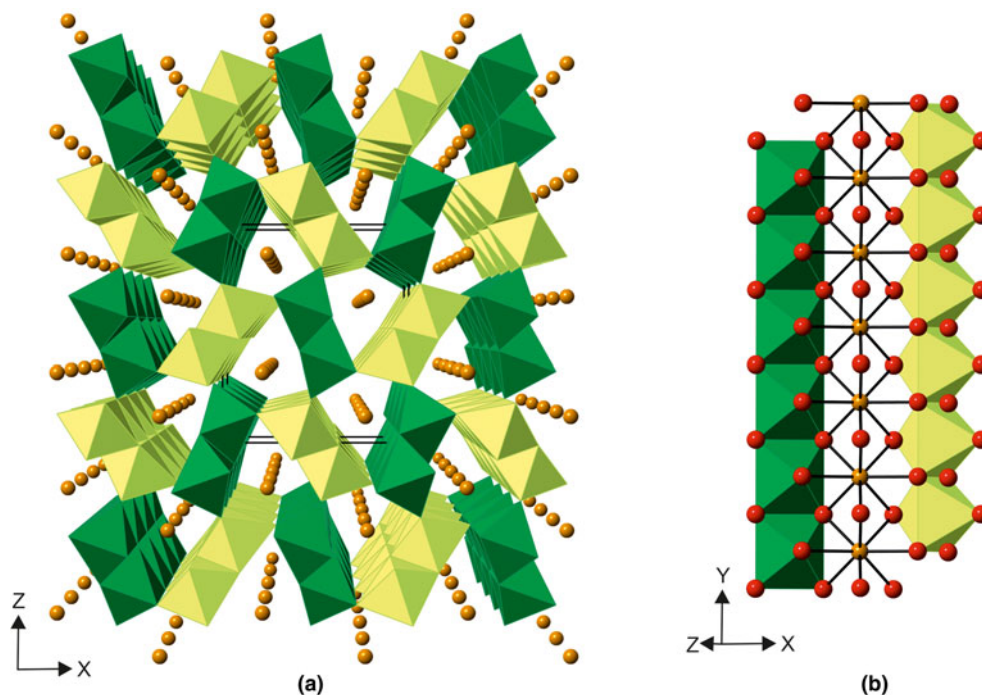


Fig. 5. (a) Ellinaite post-spinel structure, projection perpendicular to the tunnel direction (different octahedral sites are CrM1 = light-green and CrM2 = dark-green, Ca sites drawn in orange). (b) Ca sites (orange balls) in tunnel coordinated by O (red). Rutile-like chains of two types of octahedra: CrM1 (light-green) and CrM2 (dark-green) are shown.

Siwaqa area (Sokol *et al.*, 2017), whereas Cu, probably, comes from primary sulfides of the pyrometamorphic rocks.

There is a discrepancy with the temperature of varicoloured marble formation. On the basis of mineral paragenesis it was

determined to be 800–850°C (Khoury *et al.*, 2016); however temperatures of 1000–1300°C are proposed for the holotype ellinaite formation in gehlenite pyrometamorphic rocks (Sharygin, 2019). This question has been discussed, considering conditions of priscillagrewite-(Y) formation, for which a temperature of crystallisation ~1000°C was proposed (Galuskina *et al.*, 2021).

Natural fires are non-equilibrium processes, and it is expected that a local increase of temperature for a short duration near gaseous channels penetrating the rock have taken place. These fluctuations of temperature are not reflected in alteration of the whole-rock composition, but can be decisive in the formation of μm -sized crystals of rare minerals. We consider that ellinaite and mcconnellite of varicoloured marble are formed at temperatures ~1000°C as a result of transformations of earlier minerals in the pyrometamorphic rocks.

There are no doubts that the structural data obtained for the holotype ellinaite from Israel needs further verification, although it is necessary to underline that experimental data on the composition and Raman spectroscopy (Sharygin, 2019; Sharygin *et al.*, 2020) point out that this is a phase analogous to the synthetic post-spinel $\beta\text{-CaCr}_2\text{O}_4$.

We interpret that the holotype mcconnellite described by Milton *et al.* (1976) from the hydrated ore of Guyana should be re-investigated using modern methods. Mcconnellite belongs to the 3R polytype of CuCrO_2 and a synthetic polytype 2H is also known (hexagonal, $P63/mmc$ (No. 194), $a = 2.9740(3)$ Å, $c = 11.400(1)$ Å, $V = 87.3$ Å³ and $Z = 2$, Grotz and Kubel, 1996, Fig. 7). Mcconnellite was described as a Cu-enriched zone in grimaldiite, CrOOH ($R\bar{3}m$, $a = b = 2.973(2)$ and $c = 13.39(1)$ Å) (Milton *et al.*, 1976). Taking into consideration the similarity of octahedral layers in grimaldiite, two polytypes of CuCrO_2 that are defined by their oriented intergrowths, and also the conformity of powder X-ray diffraction patterns, accurate determination of the holotype mcconnellite structure is needed. Experimental data indicate that the polytype

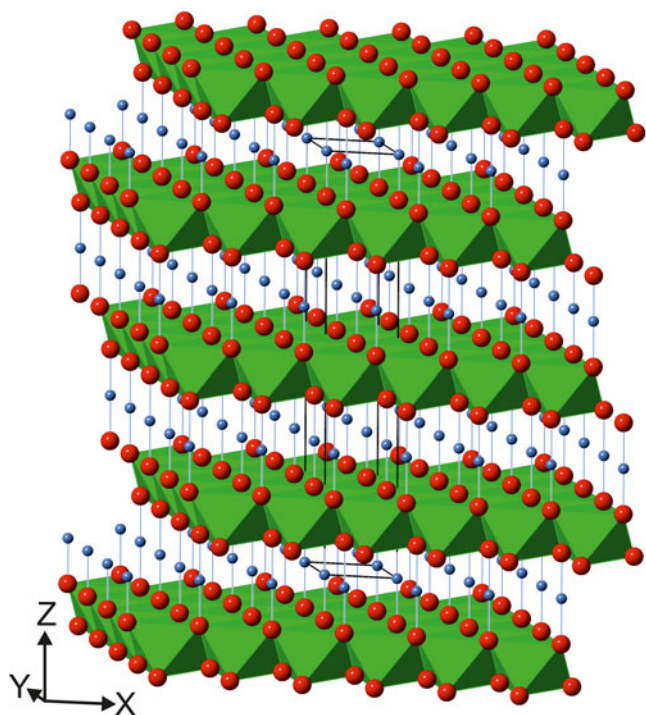


Fig. 6. Mcconnellite structure formed by octahedral layers $(\text{CrO}_2)^+$, linked together by Cu^+ cations. Cu – blue balls, CrO_6 – green octahedra and oxygen – red balls.

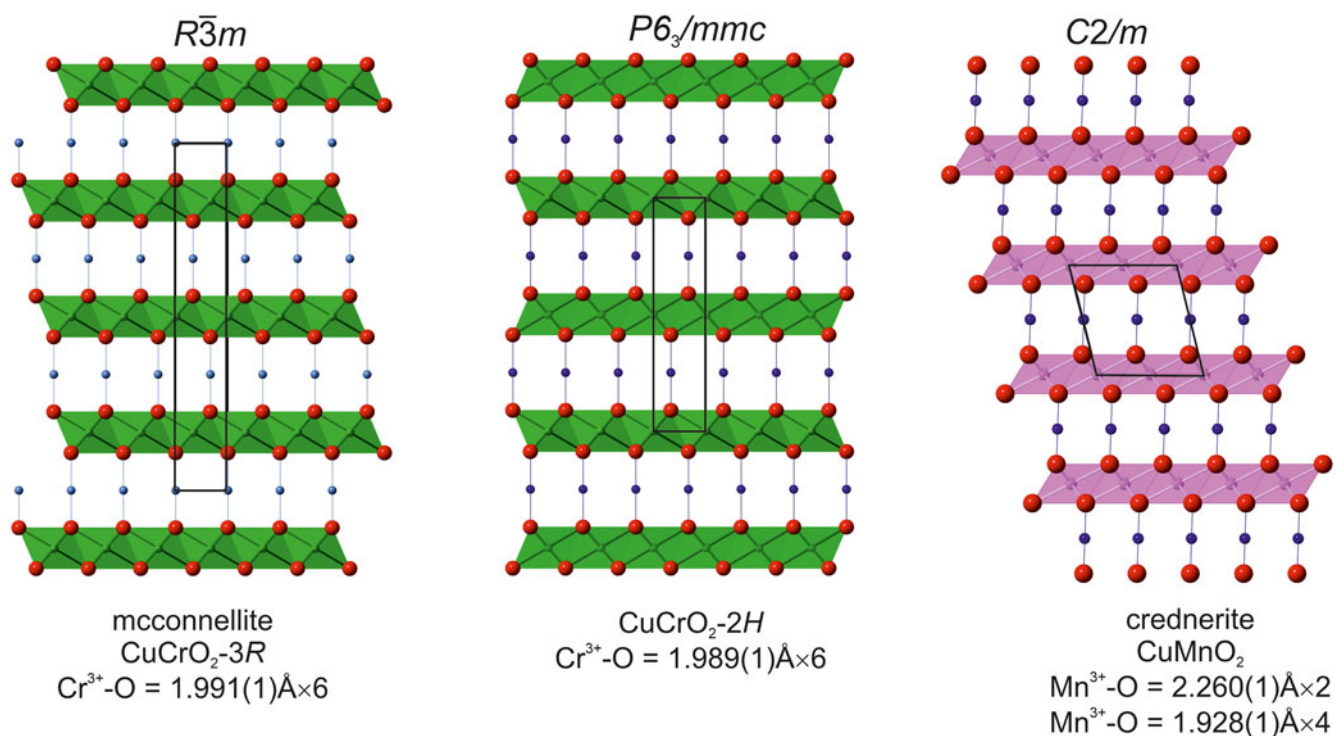


Fig. 7. Comparison of two structures of the $CuCrO_2$ polytypes – $3R$ (our data) and $2H$ (Grotz and Kubel, 1996) with the crednerite structure (Töpfer *et al.*, 1995), in which trioctahedral layers are formed by strongly deformed octahedra ($Mn^{3+}O_6$). All projections on (010). $Cr^{3+}O_6$ – green, $Mn^{3+}O_6$ – pink, Cu – blue balls and O – red balls.

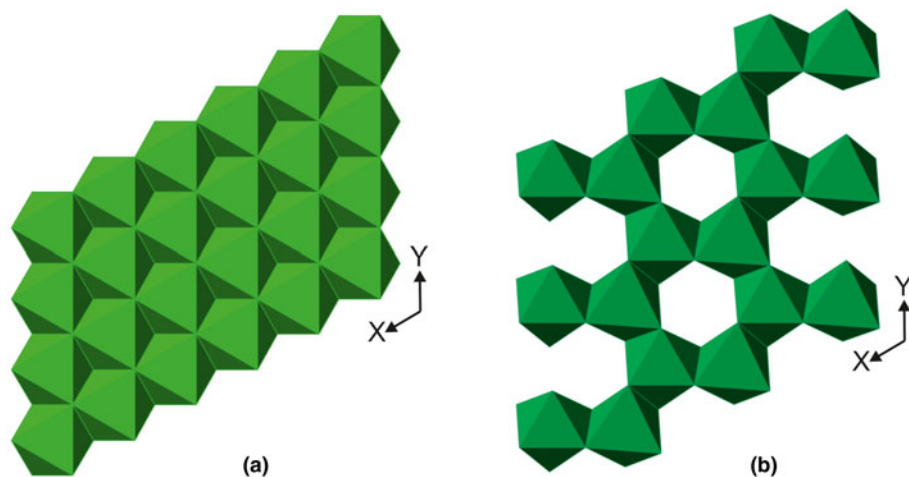


Fig. 8. (a) Trioctahedral layer in mcconnellite, $CuCrO_2$; and (b) dioctahedral layer in eskolaite, Cr_2O_3 .

$CuCrO_2-2H$ is a lower temperature phase compared to $CuCrO_2-3R$ (Miclau *et al.*, 2012). There is a possibility that the holotype mcconnellite is not a separate mineral species but corresponds to grimaldiite enriched in copper.

Except delafossite ($R\bar{3}m$, $a = 3.02-3.04$ and $c = 17.10-17.12$; Pabst, 1946) which is isostructural with mcconnellite, only one structurally related mineral – crednerite, $CuMnO_2$ ($C2/m$, $a = 5.578(6)$, $b = 2.881(2)$ and $c = 5.886(7)$ Å; Töpfer *et al.*, 1995), is known in Nature. Crednerite does not have three-fold symmetry as a result of the Jahn–Teller effect of Mn^{3+} (Fig. 7).

In conclusion, we would like to dwell on a problem related to mcconnellite. In the Raman spectra of mcconnellite from Jordan, there is a strong band at $537-538\text{ cm}^{-1}$, and a shoulder

at $556-558\text{ cm}^{-1}$ (Fig. 4), which also appears in the Raman spectra of synthetic analogues (Aktas *et al.*, 2012; Monteiro *et al.*, 2017). Additionally, if the other strong bands at 458 cm^{-1} (Eg) and 709 cm^{-1} ($Ag1$) are related to the Raman selection rule, then the band at $537-538\text{ cm}^{-1}$ (and the shoulder at $556-558\text{ cm}^{-1}$) breaks this rule and they are connected with structural defects (Majee and Bhoje, 2020; Han *et al.*, 2020). In eskolaite, Cr_2O_3 , the main band at $\sim 548\text{ cm}^{-1}$ is related to the symmetric stretching vibrations of Cr–O in (CrO_6) octahedra (Shim *et al.*, 2004), i.e. only 10 cm^{-1} lower than in mcconnellite (Fig. 4). In the mcconnellite structure, the layers are trioctahedral, whereas in the eskolaite structure they are dioctahedral (Fig. 8). Most likely, the strong band at $537-538\text{ cm}^{-1}$ in mcconnellite results from

the Cr–O stretching symmetric vibrations, and the shoulder at 556–558 cm^{-1} – from the Cr–O asymmetric vibrations in (CrO_6) octahedra connected with defects of eskolaite type in the $(\text{CrO}_2)^-$ octahedral layer.

Acknowledgements. The investigations were partially supported by the National Science Centre (NCN) of Poland, grant no. 2016/23/B/ST10/00869 (EG, IG). KW acknowledges a financial support within the Polish National Science Centre (NCN) OPUS17 no. 2019/33/B/ST10/02671. We are grateful to Viktor Sharygin for providing additional data on the holotype ellinaite. We thank two anonymous referees for constructive comments that help to improve the first version of the manuscript.

Supplementary material. To view supplementary material for this article, please visit <https://doi.org/10.1180/mgm.2021.27>.

References

- Aktas O., Truong K.D., Otani T., Balakrishnan G., Clouter M.J., Kimura T. and Quirion T. (2012) Raman scattering study of delafossite magnetoelectric multiferroic compounds: CuFeO_2 and CuCrO_2 . *Journal Physics: Condensed Material*, **24**, 036003.
- Brown I. and Altermatt D. (1985) Bond-valence parameters obtained from a systematic analysis of the inorganic crystal structure database. *Acta Crystallographica*, **B41**, 244–247.
- Dannhauser W. and Vaughan P.A. (1955) The crystal structure of cuprous chromite. *Journal of the American Chemical Society*, **77**, 896–897.
- Dolomanov O.V., Bourhis L.J., Gildea R.J., Howard J.A.K. and Puschmann H. (2009) OLEX2: a complete structure solution, refinement and analysis program. *Journal of Applied Crystallography*, **42**, 339–341.
- Elkhouni T., Amami A., Strobel P. and Ben Salah A. (2013) Structural, Raman spectroscopy, and magnetic ordering in new delafossite-type oxide $\text{CuCr}_{1-x}\text{Ti}_x\text{O}_2$ ($0 \leq x \leq 0.1$). *Journal of Superconductivity and Novel Magnetism*, **26**, 2795–2802.
- Ettler V., Johan Z., Křibek B., Šebek O. and Mihaljevič M. (2009) Mineralogy and environmental stability of slags from the Tsumeb smelter, Namibia. *Applied Geochemistry*, **24**, 1–15.
- Galuskin E.V., Gfeller F., Galuskina I.O., Pakhomova A., Armbruster T., Vapnik Y., Włodyka R., Dzierżanowski P. and Murashko M. (2015) New minerals with a modular structure derived from hatrurite from the pyrometamorphic Hatrurim Complex. Part II. Zadovite, $\text{BaCa}_6[(\text{SiO}_4)(\text{PO}_4)](\text{PO}_4)_2\text{F}$ and arditite, $\text{BaCa}_6[(\text{SiO}_4)(\text{VO}_4)](\text{VO}_4)_2\text{F}$, from paralavas of the Hatrurim Basin, Negev Desert, Israel. *Mineralogical Magazine*, **79**, 1073–1087.
- Galuskin E.V., Krüger B., Krüger H., Blass G., Widmer R. and Galuskina I.O. (2016) Wernerkrauseite, $\text{CaFe}_2\text{Mn}^{4+}\text{O}_6$ – the first non-stoichiometric post-spinel mineral, from Bellerberg volcano, Eifel, Germany. *European Journal of Mineralogy*, **28**, 485–493.
- Galuskin E., Galuskina I., Vapnik Y. and Murashko M. (2020) Molecular Hydrogen in Natural Mayenite. *Minerals*, **10**, 560.
- Galuskina I., Vapnik Y., Lazić B., Armbruster T., Murashko M. and Galuskin E. (2014) Harmunite, CaFe_2O_4 – a new mineral from the Jabel Harmun, West Bank, Palestinian Autonomy, Israel. *American Mineralogist*, **99**, 965–975.
- Galuskina I.O., Galuskin E.V., Pakhomova A.S., Widmer R., Armbruster T., Krüger B., Grew E.S., Vapnik Y., Dzierżanowski P. and Murashko M. (2017) Khesinite, $\text{Ca}_4\text{Mg}_2\text{Fe}_{10}^{3+}\text{O}_4[(\text{Fe}_{10}^{3+}\text{Si}_2)\text{O}_{36}]$, a new rhönite-group (sapphirine supergroup) mineral from the Negev Desert, Israel – natural analogue of the SFCA phase. *European Journal of Mineralogy*, **29**, 101–116.
- Galuskina I., Galuskin E., Vapnik Y., Zeliński G. and Prusik K. (2021) Priscillagrewite-(Y), $(\text{Ca}_2\text{Y})\text{Zr}_2\text{Al}_3\text{O}_{12}$ – a new garnet of the bitikleite group from the Daba-Siwaqa area, the Hatrurim Complex, Jordan. *American Mineralogist*, **106**, 641–649.
- Grottaz O. and Kubel F. (1996) Crystal structure of copper(I) chromium(III) oxide, 2H-CuCrO_2 . *Zeitschrift für Kristallographie – Crystalline Materials*, **211**, <https://doi.org/10.1524/zkri.1996.211.7.481>
- Han M., Lu Y., Liu Y., Hu Z., Chen C., Jiang K., Zhang J. and Li W. (2020) Raman scattering measurements of phonon anharmonicity in the delafossite $\text{CuGa}_{1-x}\text{Cr}_x\text{O}_2$ ($0 \leq x \leq 1$) films. *Journal of Raman Spectroscopy*, **2020**, 1–9.
- Juroszek R., Krüger H., Galuskina I., Krüger B., Ježak L., Ternes B., Wojdyla J., Krzykawski T., Pautov L. and Galuskin E. (2018a) Sharyginite, $\text{Ca}_3\text{TiFe}_2\text{O}_8$, A new mineral from the Bellerberg Volcano, Germany. *Minerals*, **8**, 308.
- Juroszek R., Krüger B., Banasik K., Vapnik Y. and Galuskina I. (2018b) Raman spectroscopy and structural study of baryte-hashemite solid solution from pyrometamorphic rocks of the Hatrurim Complex, Israel. *Spectrochimica Acta*, **A205**, 582–592.
- Juroszek R., Krüger B., Galuskina I., Krüger H., Vapnik Y. and Galuskin E. (2020a) Siwaqaite, $\text{Ca}_6\text{Al}_2(\text{CrO}_4)_3(\text{OH})_{12} \cdot 26\text{H}_2\text{O}$, a new mineral of the ettringite group from the pyrometamorphic Daba-Siwaqa complex, Jordan. *American Mineralogist*, **105**, 409–421.
- Juroszek R., Krüger B., Galuskina I., Krüger H., Tribus M. and Kürsten, C. (2020b) Raman spectroscopy and single-crystal high-temperature investigations of bentorite, $\text{Ca}_6\text{Cr}_2(\text{SO}_4)_3(\text{OH})_{12} \cdot 26\text{H}_2\text{O}$. *Minerals*, **10**, 38.
- Kaminsky F.L., Wirth R. and Schreiber A. (2015) A microinclusion of lower-mantle rock and other minerals and nitrogen lower-mantle inclusions in a diamond. *The Canadian Mineralogist*, **53**, 83–104.
- Khoury H.N. (2020) Geochemistry of rare earth elements (REE) and redox sensitive elements (RSE) of pyrometamorphic rocks, central Jordan. *Arabian Journal of Geosciences*, **13**, 174.
- Khoury H.N., Sokol E.V., Kokh S.N., Seryotkin Y.V., Nigmatulina E.N., Goryainov S.V., Belogub E.V. and Clark I.D. (2016) Tululite, $\text{Ca}_{14}(\text{Fe}^{3+}, \text{Al})(\text{Al}, \text{Zn}, \text{Fe}^{3+}, \text{Si}, \text{P}, \text{Mn}, \text{Mg})_{15}\text{O}_{36}$: a new Ca zincate-aluminate from combustion metamorphic marbles, central Jordan. *Mineralogy and Petrology*, **110**, 125–140.
- Kim J.-H., Kim J.Y., Choi, Y.H. and Youn D.H. (2020) Facile CuFeO_2 microcrystal synthesis for lithium ion battery anodes via microwave heating. *Journal of Materials Science: Materials in Electronics*, **31**, 9408–9414.
- Kolev, N., Iliev, M.N., Popov, V.N. and Gospodinov, M. (2003) Temperature-dependent polarized Raman spectra of CaFe_2O_4 . *Solid State Communication*, **128**, 153–155.
- Krzatąła A., Panikorovskii T., Galuskina I. and Galuskin E. (2018) Dynamic disorder of Fe^{3+} ions in the crystal structure of natural barioferrite. *Minerals*, **8**, 340.
- Kumar, S., Marinel, S., Miclau M. and Martin C. (2012) Fast synthesis of CuCrO_2 delafossite by monomode microwave heating. *Materials Letters*, **70**, 40–43.
- Majee M.K. and Bhobe, P.A. (2020) Correlation of local crystal structural and physical properties of the delafossite $\text{CuCr}_{1-x}\text{Fe}_x\text{O}_2$ ($0 \leq x \leq 1$). *Inorganic Chemistry*, **59**, 6790–6799.
- Miclau M., Ursu D., Kumar, S. and Grozescu, I. (2012) Hexagonal polytype of CuCrO_2 nanocrystals obtained by hydrothermal method. *Journal of Nanoparticle Research*, **14**, 1110.
- Milton C., Appleman D.E., Appleman M.H., Chao E.C.T., Cuttitta F., Dinnin J.I., Dwornik E.J., Ingram B.L. and Rose Jr., H.J. (1976) Merumite – a complex assemblage of chromium minerals from Guyana. *U.S. Geological Survey Professional Paper*, **887**, 1–29.
- Monteiro J.F.H.L., Jurelo A.R. and Siqueira E.C. (2017) Raman spectroscopy of the superconductor CuCrO_2 delafossite oxide. *Solid State Communications*, **252**, 64–67.
- Monteiro J.F.H.L., Siqueira E.C., Vallis D.S., de Andrade E., Barcote M.V.W. and Jurelo, A.R. (2018) Raman spectroscopy of (Fe,Li)-doped delafossite oxide CuCrO_2 . *Vibrational Spectroscopy*, **98**, 77–81.
- Novikov I., Vapnik Ye. and Safonova I. (2013) Mud volcano origin of the Mottled Zone, South Levant. *Geoscience Frontiers*, **4**, 597–619.
- Pabst A. (1946) Notes on the structure of delafossite. *American Mineralogist*, **31**, 539–546.
- Picard L. (1931) *Geological Research in the Judean Desert*. Goldberg Press, Jerusalem, 108 pp.
- Seryotkin Y.V., Sokol E.V., Kokh S.N. and Sharygin V.V. (2019) Natural bentorite- Cr^{3+} derivate of ettringite: determination of crystal structure. *Physics and Chemistry of Minerals*, **46**, 553–570.
- Shannon R.D. (1976) Revised effective ionic radii and systematic studies of interatomic distances in halides and chalcogenides. *Acta Crystallographica*, **A32**, 751–767.
- Sharygin V.V. (2019) Orthorhombic CaCr_2O_4 in phosphide-bearing gehlenite-rankinite paralava from Hatrurim Basin, Israel: preliminary data. *Conference materials: Magmatism of the Earth and Related Strategic Metal Deposits*, **36**, 272–276.
- Sharygin V.V., Lazić B., Armbruster T.M., Murashko M.N., Wirth R., Galuskina I.O., Galuskin E.V., Vapnik Y., Britvin S.N. and Logvinova

- A.M. (2013) Shulamitite, $\text{Ca}_3\text{TiFe}^{3+}\text{AlO}_8$ – a new perovskite-related mineral from Hatrurim Basin, Israel. *European Journal of Mineralogy*, **25**, 97–111.
- Sharygin V.V., Britvin S.N., Kaminsky F.V., Wirth R., Nigmatulina E.N., Yakovlev G.A., Novoselov K.A. and Murashko, M.N. (2020) Ellinaite, IMA 2019-091. CNMNC Newsletter No. 53; *Mineralogical Magazine*, **84**, <https://doi.org/0.1118/gm.2020.5>
- Sheldrick G.M. (2015a) SHELXT – Integrated space-group and crystal-structure determination. *Acta Crystallographica*, **A71**, 3–8.
- Sheldrick G.M. (2015b) Crystal structure refinement with SHELXL. *Acta Crystallographica*, **C71**, 3–8.
- Shim S.-H., Duffy T.S., Jeanloz R., Yoo C.-S. and Iota V. (2004) Raman spectroscopy and X-ray diffraction of phase transitions in Cr_2O_3 to 61 GPa. *Physical Review*, **B69**, 144107.
- Sokol E.V., Gaskova O.L., Kokh S.N., Kozmenko O.A., Seryotkin Y.V., Vapnik Y. and Murashko M.N. (2011) Chromatite and its Cr^{3+} - and Cr^{6+} -bearing precursor minerals from the Nabi Musa Mottled Zone complex, Judean Desert. *American Mineralogist*, **96**, 659–674.
- Sokol E.V., Kozmenko O.A., Khoury H.N., Kokh S.N., Novikova S.A., Nefedov A.A., Sokol I.A. and Zaikin P. (2017) Calcareous sediments of the Muwaqqar Chalk Marl Formation, Jordan: Mineralogical and geochemical evidences for Zn and Cd enrichment. *Gondwana Research*, **46**, 204–226.
- Stroupe J.D. (1949) An X-ray diffraction study of the copper chromites and of the “copper-chromium oxide” catalyst. *Journal of the American Chemical Society*, **71**, 569–572.
- Töpfer J., Trari M., Gravereau P., Chaminade J.P. and Doumerc J.P. (1995) Crystal growth and reinvestigation of the crystal structure of crednerite, CuMnO_2 . *Zeitschrift für Kristallographie*, **210**, 184–187.
- Zhai S., Yin Y., Shieh S.R., Shan S., Xue W., Wang C.-P., Yang, K. and Higo Y. (2016) High-pressure X-ray diffraction and Raman spectroscopy of CaFe_2O_4 -type $\beta\text{-CaCr}_2\text{O}_4$. *Physics and Chemistry of Minerals*, **43**, 307–314.